Nanotechnology for Environmental Engineering (2023) 8:49–62
https://doi.org/10.1007/s41204-022-00268-8

ORIGINAL PAPER

Behavior of the adsorption of Allura Red dye by chitosan beads and nanoparticles

Sánchez-Duarte Reyna G.[1] · Villegas-Peralta Yedidia[1] · Martínez-Macias María del Rosario[1] · López-Cervantes Jaime[2] · Sánchez-Machado Dalia I.[2] · Correa-Murrieta Ma. A.[1]

Received: 5 January 2022 / Accepted: 7 June 2022 / Published online: 4 July 2022

Abstract

In this study, the adsorption capacity of Allura Red (AR) dye by chitosan cross-linked tripolyphosphate beads (BCS) and nanoparticles (CSNPS) was compared. The adsorbents were characterized by FTIR, SEM, TEM, SD, and pH_{pzc}. The evaluation of adsorption parameters was carried out in a batch processing system and under acidic conditions, using kinetics and adsorption isotherms models. Pseudo-first-order, pseudo-second-order, and intraparticle diffusion kinetic models were analyzed. The experimental adjusted data were compared to the Langmuir, Freundlich, Dubinin–Raduskevich, Tempkin, and Redlich–Peterson adsorption models using the coefficient of determination (R^2) for the linear and nonlinear methods, and the chi-square value (χ^2) for the nonlinear method. FTIR confirmed the sodium tripolyphosphate (TPP) cross-linking and the AR adsorption. The surface morphology observed by SEM was similar for both adsorbents. The diameter of CSNPS (27.64 nm ± 0.05 nm) was smaller than the beads (2.23 ± 0.248 mm). The CSNPS showed the highest swelling degree (127.265%), and the behavior pH_{pzc} for CSNPS and BCS was equivalent to 4.8 and 4.7, respectively. The results of adsorption kinetics showed that the chemisorption governs the AR adsorption process on both adsorbents (BSC and CSNPS). The best-fitting isotherm models for the adsorption of AR on CSNPs and BCS were Tempkin and Langmuir, respectively. The CSNPS showed a higher adsorption capacity (370.37 mg g^{-1}) than the BCS (13.60 mg g^{-1}) because of their smaller particle size, which increases the adsorption capacity and reduces the time to reach adsorption equilibrium.

Keywords Kinetics · Isotherms · Chitosan · Nanoparticles · Beads

Introduction

A high population growth rate, the over-exploitation of natural resources, and the immoderate use of chemical products have caused a strain on the planet's natural resources and its ability to support a growing human population. Among the range of products increasingly used in the food, chemical, pharmaceutical, and cosmetic industries are dyes. These industries use more than 100,000 commercial dyes and approximately 10,000 tons, per year [1, 2].

Approximately 10–50% of the total amount of reactive dyes remain in the effluent after the dyeing processes are completed [3, 4]. Dyes in water can be toxic, recalcitrant, potential carcinogens and can cause visible damage to the environment. If released to the environment without a proper management, they may also affect the health of all living organisms [5]. In order to minimize the contamination of water with dyes and to ensure the quality of the discharged water, it is necessary to know the contamination source, its characteristics, and applied treatments [6]. Flocculation, adsorption, redox processes, biological degradation, and membrane separation are among the methods being used to remove dyes from water [7]. However, the adsorption technique using low-cost adsorbents is one of the most efficient and financially viable [8]. Furthermore, it is well known that this technique provides better results than commercially

✉ Villegas-Peralta Yedidia
Yedidia.villegas@itson.edu.mx

✉ Martínez-Macias María del Rosario
maria.martinez@itson.edu.mx

[1] Departamento de Ciencias del Agua y Medio Ambiente, Instituto Tecnológico de Sonora, 5 de febrero 818 Sur, 85000 Ciudad Obregón, Sonora, Mexico

[2] Departamento Biotecnología y Ciencias Alimentarias, Instituto Tecnológico de Sonora, 5 de febrero 818 Sur, 85000 Ciudad Obregón, Sonora, Mexico

available adsorbents because of their ability to be regenerated, resulting in a lower cost to benefit rate [9].

Chitosan is a natural biopolymer originated from the deacetylation of chitin in the exoskeleton of crustaceans such as shrimp, crab, lobster, and squid [10]. Chitosan is an excellent, low-cost adsorbent, whose global industrial production relies on the use of shrimp shell scrap. Numerous studies have been published emphasizing the chemical compounds that can improve the adsorbent qualities of chitosan by adding new functional groups [6], for example, glutaraldehyde, sodium alginate, sodium tripolyphosphate, and epichlorohydrin. Sodium tripolyphosphate (TPP) is a multivalent polyanion and water-soluble agent with a low toxicity, it can interact with its phosphates groups ($P_3O_{10}^{5-}$) with the cationic chitosan ($NH3^+$) by electrostatic force to improve chitosan characteristics [11, 12]. Hence, pure, and improved forms of chitosan (microparticles, nanoparticles, beads, and membranes) have been prepared and widely used for the adsorption of a great variety of dyes.

For example, Hasan et al. [13] studied chitosan as an adsorbent for the removal of acid dyestuff, namely acid green 25, acid orange 10, acid orange 12, acid red 18, and acid red 73 from aqueous solution resulting in adsorption capacities of 640–730 mg g^{-1}. Foruzin et al. [14] removed Congo red dye using chitosan-TPP nanoparticles with a maximum encapsulation efficiency of 5107 mg g^{-1}. The reports made by Bevziuk et al. [15] showed that orange II dye and methylene blue were removed by using magnetic calcium-modified chitosan microparticles in aqueous solution reached to 350–962 mg g^{-1} adsorption capacity. Sadegh et al. [16] by using functionalized chitosan nanocomposites adsorbed methyl orange and Congo red acquiring an adsorption capacity of 551.2 and 274.7 mg g^{-1}. Such studies demonstrated the use of derived of chitosan in removing dyes is possible and likely to be a good option. Although there is a wide variety of dyes, azo dyes are the main industrially synthesized organic-colored compounds, and they have the particularity to contain one or more azo groups (N=N). These dyes are used as coloring agents in the cosmetic, textile, plastic, paint, paper, food, and pharmaceutical areas. One of the dyes mostly used in the industries is Allura Red, which is an azoic type of colorant, and has been proven in previous studies that it is carcinogenic and mutagenic [17]. Due to its azo structure is a risk to the human being as it has been confirmed to possess clear toxic effects on the liver and kidney of humans, likewise the discharge of Allura Red to bodies of water can bring about numerous environmental problems coloration and low oxygenation [18], hence the importance of treating this contaminant. Table 1 shows a list of adsorbents and its adsorption capacity for Allura Red dye.

The research studies listed above present very varied ranges of adsorption capacities for Allura Red dye and some of them with very expensive techniques to be produced, most of which consider linear methods and describe one single adsorbent. This study analyzes and compares the behavior of adsorption of Allura Red (AR) dye using beads and nanoparticles of chitosan cross-linked with sodium tripolyphosphate in a batch system. Kinetics studies were used to correlate the experiments based on the pseudo-first-order, pseudo-second-order, and intraparticle diffusion models. In addition, the modeling of the adsorption behavior was carried out using the Langmuir, Freundlich, Dubinin–Radushkevich, Tempkin y Redlich Peterson isotherms models. This study is further to clarify the adsorption of Allura Red dye as a water pollutant on chitosan adsorbents and this could be applied in real-life situations.

Experimental

Materials

Chitosan was obtained and characterized in previous studies by Ávila-Martínez et al. [21]. It was derived by alkaline deacetylation of chitin contained in shrimp shells, at a 92.16% degree of deacetylation, a molecular weight of 3.16×10^5 g $gmol^{-1}$, and 5.64 ± 0.045% of moisture content. Allura Red dye (AR) at 80% CI 16,035; molecular

Table 1 Comparison of adsorbents used for Allura Red dye

Adsorbent	Adsorption capacity	References
Activated carbon produced from peanut hulls	28.36 mg L^{-1}	Torres-Perez [2]
Silver nanoparticles deposition on silica, magnetite, and alumina surfaces	71.68 mg g^{-1}	Salem et al. [7]
Activated charcoal based on walnut shells	9.990 mg g^{-1}	Herrera-García et al. [19]
Biosponges of Luffa-glutaraldehyde and Luffa-epichlorohydrin with chitosan	89.05 mg g^{-1}	Schio et al. [20]
	60.91 mg g^{-1}	
Zirconia fibers	0.895 mg g^{-1}	Blackburn, Harvey [3]
Activated carbon from carboxymethyl cellulose	223.2 mg g^{-1}	Wang et al. [18]
Chitosan nanoparticles and beads cross-linked with Sodium Tripolyphosphate	370.37 mg g^{-1}	This work
	13.60 mg g^{-1}	

weight = 496.42 g mol^{-1} was purchased from Sigma-Aldrich and used as the adsorbate.

Sodium tripolyphosphate (TPP: $Na_5P_3O_{10}$) 85% reagent grade, sodium hydroxide (NaOH) 97% reagent grade, and hydrochloric acid (HCL) 98% were obtained from Sigma-Aldrich (St. Louis, MO, USA). Glacial acetic acid (CH_3COOH) 99.5% reagent grade was acquired from Fermont (Monterrey, Mexico). Standard solutions of 0.1 N sodium hydroxide (NaOH), 0.1 N hydrochloric acid (HCL) and 0.1 N sodium chloride (NaCl) were used to adjust the pH.

Adsorbents characterization

Chitosan beads (BCS) and chitosan nanoparticles (CSNPS), both TPP cross-linked, were prepared in accordance with previous studies conducted by Sánchez-Duarte et al. [22] and Villegas-Peralta, et al. [23], respectively. The method for the preparation of CSNPS consisted in the mixture of two solutions. A solution of 0.14% TPP was poured in a 0.2% chitosan solution (10 mL/min) under agitation. Later the mixed solution was frozen and centrifuged at 6000 rpm with two repeated washes and then was lyophilized (Lab Conco Free zone 1). The method for production of cross-linked chitosan tripolyphosphate beads (BCS) is described to continuation. Briefly, a solution of chitosan (1.5 wt%) was added drop by drop from a pipette into an aqueous solution of TPP (1 wt%) in a relation 1:10, then the formation of spherical beads of chitosan tripolyphosphate (BCS) was spontaneously. Figure 1 shows the sequence of preparation of beads and nanoparticles by using a photographic scheme.

Functional groups of the adsorbents were taken with Fourier transform infrared spectroscopy (FTIR) in a range of 4000–400 cm^{-1} (Thermo Scientific Spectrum model Nicolet iS5). An accessory of transmission iD1 was used to collect the sample. The OMNIC software was used to manipulate the data. SEM images were obtained by using a scanning electron microscope (HR-SEM, JEOL JSM-7600F, 15 kV, 25,000×), EVO LS 15 (Carl Zeiss SMT, 25 kV, 3790×) for CSNPS and BCS, respectively. A transmission electron microscope (TEM, JEOL JEM-2010) operated at 200 kV was utilized to measure the diameter of the nanoparticles and a digital Vernier calipter (Fisher Scientific, Mexico) was used to determine the diameter of beads.

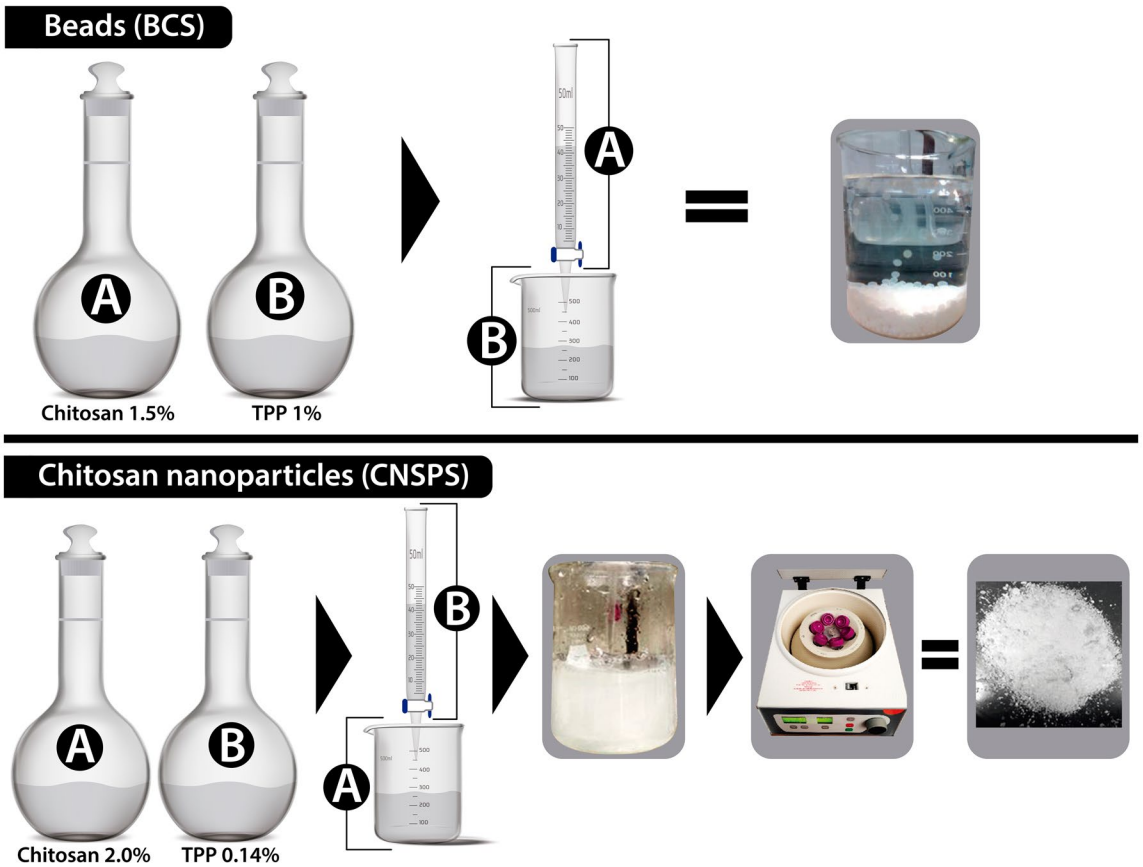

Fig. 1 Sequence of preparation of nanoparticles chitosan cross-linked with sodium tripolyphosphate (CSNPS) and beads chitosan cross-linked with sodium tripolyphosphate (BCS)

The point zero charge (pH_{pzc}) of the adsorbents was analyzed through a drift method of Sharma et al. [24]. pH solutions were prepared in a range of 2–11, by using a 50 mL Falcon tube with the help of HCl (0.1 N) and NaOH (0.1 N). Then, to each tube, 25 mL of NaCl was added under nitrogen atmosphere to avoid CO_2 interferences. A mass of 0.05 g sample was then added. After that, the tubes were placed in an incubator during 24 h at 120 rpm. At the end of the cycle, the pH was measured and registered as final pH. A plot of initial (X) and final pH (Y) was created, the value of ΔpH where the charge was zero was taken as pH_{pzc}.

The swelling degree (SD) was obtained by following the method described by Gonçalves et al. [25] and Sharma et al. [26]. A mass of adsorbent (5 mg) was submerged in distillated water, and it was kept under constant agitation during 24 h at 120 rpm and 25 °C. Equation 1 is applied to determine the swelling degree; where M_i is the weight of the initial mass and M_f is the weight after the water contact.

$$\%\text{Swelling} = \left(\frac{M_i - M_f}{M_i}\right) \times 100 \tag{1}$$

Adsorption kinetics

Pseudo-first-order (Lagergreen), pseudo-second-order (Ho y McKay), and intraparticle diffusion (Webber and Morris) kinetic models were used to understand the adsorption processes taking place among BCS, CSNPS, and Allura Red dye. Equations and descriptions of each variable are shown in Table 2.

The concentration's range of Allura Red dye was 25–100 ppm and 10–200 ppm for beads and CNSPS, respectively. These concentrations were prepared with an optimum adsorbent mass and a pH value resulting from adsorption tests described in previous studies (pH = 4, dry weight of beads = 0.25 g and nanoparticles = 0.02 g). The dye solutions and adsorbents were mechanically stirred for various time intervals ("time of contact") until an equilibrium concentration was reached. For tests using beads, a minimum time (t_{min}) of 360 min and a maximum (t_{max}) of 720 min were used. For the test using CNSPS, t_{min} and t_{max} were 18 min and 1440 min, respectively. The concentration values used for these tests are listed in Tables 4 and 5. After the time of contact, the adsorbents were separated from the solution. The BSC were removed by decantation, while the CSNPS were separated using a microfiltration equipment (Kontes Ultra-Ware Microfiltration). The absorbance of the remaining solutions was determined using a spectrophotometer (Thermo Spectronic Genesys 20 (4001/4) at 510 nm, and the resulting value was used to calculate the final concentration (C_f in mg L^{-1}), using Eq. 5.

$$q_t = \frac{\left(C_o - C_f\right) V}{m} \tag{5}$$

where q_t is the adsorption capacity (mg g^{-1}), V represents the solution volume (L), and m is dry weight of adsorbent mass (g). The adsorption capacity resulting from the equation was used to determine the equilibrium adsorption capacity represented by q_e and expressed in mg g^{-1}. Once these values were defined, equations were applied to define the kinetic models (Table 2) and isotherm models (Table 3). Figure 2 shows the physical process to determine the removal capacity, the nanoparticles and beads after adsorption can be appreciated as well.

Adsorption isotherms

Identifying the type of adsorption in a process is crucial because it may indicate how the adsorption system is structured. It also shows how an adsorbent and adsorbate interact with each other. In this study, Allura Red dye adsorption tests were performed on BCS and CSNPS using Langmuir, Freundlich, Dubinin–Raduskevich, Tempkin, and Redlich Peterson models. The relevant equations are listed in Table 3.

Langmuir

The Langmuir isotherm (Eq. 6, Table 3) describes a gas–solid adsorption onto activated carbon. It is an empirical

Table 2 Equations and descriptions of variables of the kinetic models

Kinetic model	Equations	Variable	References
Pseudo-first-order Lagergreen	$\log\left(q_e - q\right) = \log q_e - \frac{k_1 t}{2.303}$ (2)	k_1, Lagergreen constant, min^{-1}	[27]
Pseudo-second-order Ho y McKay	$\frac{t}{q_t} = \frac{1}{k_2 q_e^2} + \frac{t}{q_e}$ (3)	k_2, Ho y McKay constant, mg min^{-1} g^{-1}	[28]
Intraparticle diffusion	$q_t = k_p t^{1/2} + B$ (4)	k_p, intraparticle diffusion constant of Webber and Morris, mg $min^{1/2}$ g^{-1}	[29]
		q_e, adsorption capacity at equilibrium, mg g^{-1}	
		q_t, dye adsorption at equilibrium, mg g^{-1}	

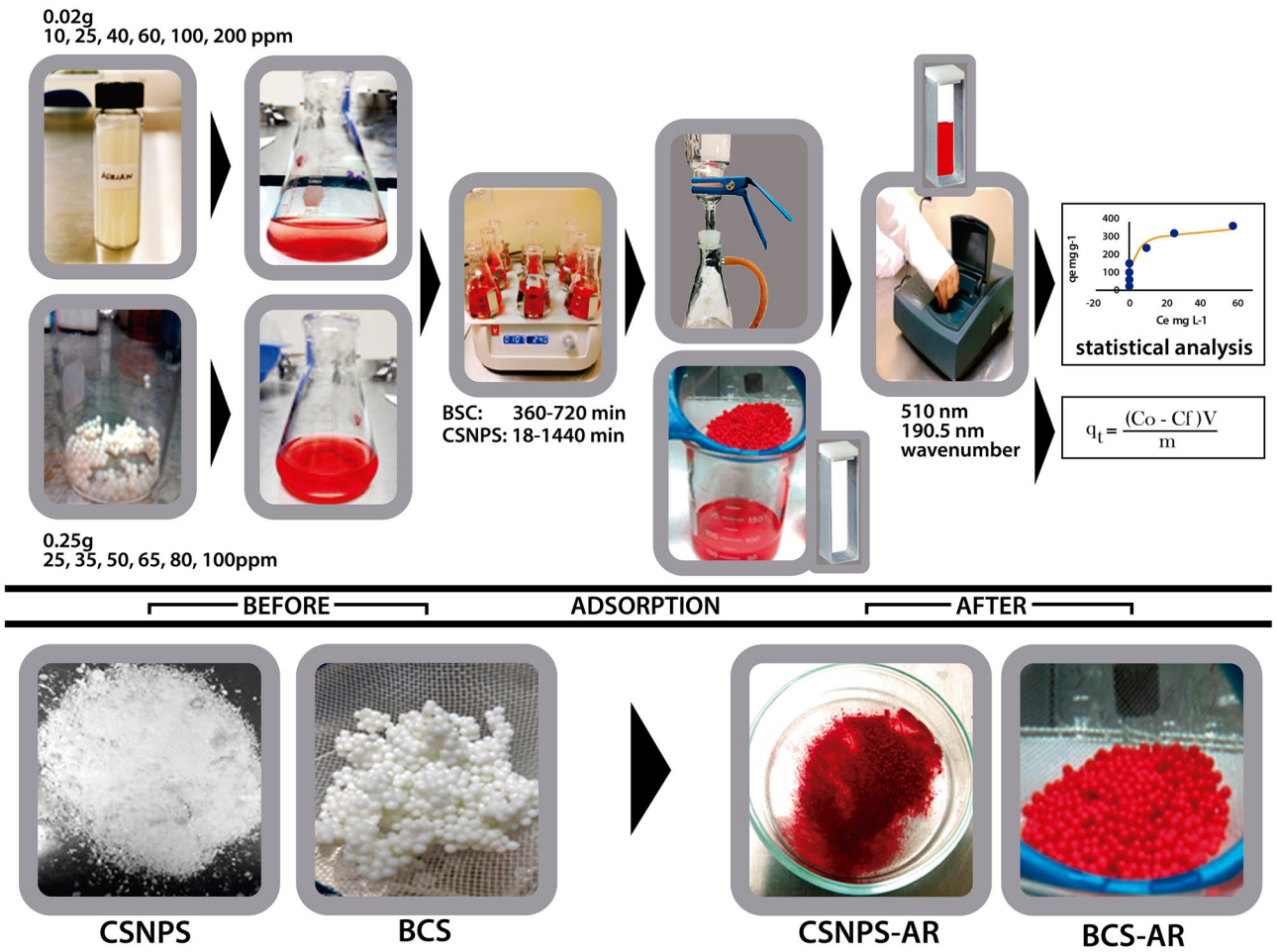

Fig. 2 Physical laboratory process to determine the removal capacity. Nanoparticles (CSNPS) and beads (BCS) before and after adsorption

Table 3 Equations and descriptions of isotherm models variables

Isotherm	Lineal form equation	Equation	Variables	References
Langmuir	$qe = \frac{q_{max} K_L C_e}{1/K_L C_e}$	(6)	C_e, dye concentration at equilibrium, mg g^{-1} k_L, Langmuir constant, L g^{-1}	[35]
Freundlich	$q_e = KfC_e^{1/n}$	(7)	q_{max}, maximum adsorption capacity, mg g^{-1} q_e, adsorption capacity at equilibrium, mg g^{-1}	[36]
Dubinin–Raduskevich	$q_e = q_s \exp\left(K_{ad}\varepsilon^2\right)$ $\varepsilon = RT \ln\left(1 + {}^1/_{C_e}\right)$ $E = \frac{1}{\sqrt{2K_{ad}}}$	(8) (9) (10)	q_s, adsorption capacity of saturation, mg g^{-1} k_{ad}, Dubinin–Raduskevich constant, mol^2/kJ^2 E, free energy, per molecule of adsorbate, kJ mol^{-1} R, gas constant, 8.314 J mol^{-1} K^{-1} T, temperature, 298.15 K	[8]
Tempkin	$qe = \frac{RT}{b_T} \ln\left(A_T C_e\right)$	(11)	b_t, Tempkin constant, kJ mol^{-1} A_t, equilibrium binding constant, L mg^{-1}	[33]
Redlich–Peterson	$q_e = \frac{K_r C_e}{1 + a_r C_e^g}$	(12)	K_r, Redlich–Peterson isotherm constants L g^{-1} a_r, Redlich–Peterson isotherm constant, (L mg^{-1}) g g, exponent Redlich–Peterson isotherm constant	[37]

Table 4 Statistical analysis

Error analysis	Equation		Variables	References
Coefficient of determination	$R^2 = \frac{\sum (q_c - \overline{q})^2}{\sum (q_c - \overline{q})^2 + \sum (q_c - q_e)^2}$	(13)	q_e, adsorption capacity at equilibrium l, mg g^{-1}	[39]
			q_c, adsorption calculated capacity using the equation of each model, mg g^{-1}	
Chi-square	$\chi^2 = \sum \frac{(q_e - q_c)^2}{q_e}$	(14)	$\overline{q}$, average adsorption capacity at equilibrium, mg g^{-1}	[40]

model that assumes that a monolayer adsorption occurs only at a limited number of locations, which are identical and equivalent, and that lateral interactions between the adsorbed molecule and adjacent sites do not occur [30].

Freundlich

The Freundlich isotherm (Eq. 7, Table 3) is an empirical equation that relates to heterogeneous adsorbent surfaces [31]. It represents a multilayer adsorption that takes place on surfaces with different adsorption energy levels [32].

Dubinin–Raduskevich

The Raduskevich equation is widely used for the interpolation of an adsorption process that takes place on a porous material and describes the mechanism with a Gaussian energy distribution [20]. The equation is shown in Eq. 8 in Table 3.

Tempkin

This isotherm (Eq. 11, Table 3) takes into consideration the interactions between the adsorbent and adsorbate. It also shows that the adsorption heat of all molecules will decrease linearly, and it is not restricted to low or high concentrations [33].

Redlich–Peterson

The equation describing the Redlich–Peterson isotherm is shown in Eq. 12 of Table 3. It is mostly used as a combination of the Langmuir and Freundlich models. The process of adsorption does not adhere to the ideal monolayer adsorption [34]. The constant g is an exponent with a value between 0 and 1. When g is closer to 1, the behavior resembles the Langmuir model. When g is closer to 0, it resembles the Freundlich isotherm.

Statistical analysis

In this study, the coefficient of determination (R^2) was used to identify the isotherm model that best fits the experimental data obtained. R^2 was calculated using linear and nonlinear methods (Eq. 13, Table 4). Chi-square χ_i^2 [38] was used to evaluate the variable isotherm models with the a nonlinear method. The information obtained was then used to compare each curve fitted to the experimental data. The software used to model the equations of adsorption was Origin Pro 9 and Microsoft Excel using its Solver complement.

Results and discussion

Adsorbents characterization

FTIR measurements were conducted to demonstrate the nature functional groups of the adsorbents, and its interaction with the cross-linker, therefore, the possible interaction between Allura Red dye after adsorption is identified. As it is shown in Fig. 3, the representation of strong peaks for CSNPS in 1636.54, 1539.01 1402.79 cm^{-1} and 1399.84, 1539.01 and 1648. 48 cm^{-1} for BCS is attributed to the C=O of the amino groups of chitosan (-CONH), the bending vibration of N–H and the O–H deformation, respectively [41]. The results of the spectra after adsorption showed

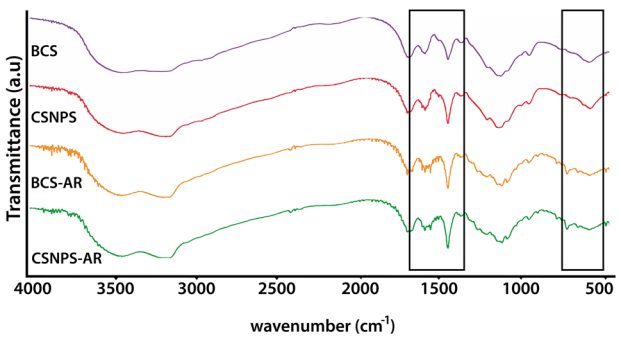

Fig. 3 FTIR spectra of the raw adsorbents (CNSPS and BCS) and after Allura Red dye adsorption (CSNPS-AR and BCS-AR)

slight displacement of the amino groups, the N–H and O–H groups but particularly new bands at 1539.01 cm^{-1} in CSNPS-AR and 1544.93 cm^{-1} in BCS-AR, these functional groups are presumed to be responsible for the adsorption of AR. Also, the peaks rising at 2376.14 and 2373.19 cm^{-1} can be presumed that the -NH_2 present in the surface of both adsorbents were reliable for binding negatively charged AR through electrostatic forces. The intense broad peak range of 3100–3200 cm^{-1} was a peculiar characteristic of the hydroxyl group (O–H) that was present at all spectra [42, 43]. The cross-linking with TPP is recognized as the band in the stretching of 515.52 and 518.48 cm^{-1} in BCS and CSNPS, respectively, which was ionically cross-linked with phosphates groups ($P=0$), a slight displacement of the phosphates groups was detected for the adsorbed spectrums, and it is attributed to the adsorption of the dye (CSNPS, 655.44 cm^{-1} and BCS, 657.51 cm^{-1}) [44].

The scanning electron microscopy technique was developed to determine the surface morphology in the adsorbents, which it is shown in Fig. 4. For BCS (Fig. 4a), it was observed micrometric size spherical particles. The surface can be interpreted as porous and with deep channels that can be related to the adsorption capacity for pollutant. For CSNPS (Fig. 4b), it is noted that the cover of the nanoparticles is homogeneous with cracks along the surface, the same performance was reported by Thirumalaikumar et al. [45] and Villegas-Peralta et al. [46]. The standardized surface behavior of CSNPS and BCS can be positively related to the capacity to adsorb the pollutant, and this is associated with adsorption capacity reported in this study (CSNPS > BCS) of both adsorbents. The diameter of the CSNPS was 27.64 nm ± 0.05 nm. This was measured by using a transmission electron microscopy. The diameter of the BCS was 2.23 ± 0.248 mm, which was determined by using a digital Vernier caliper. According to Tsotetsi et al. [47], the small size of particles is related with higher specific surface area and therefore in a high adsorption capacity.

The potential zero charge pH_{pzc} is a measurement in which a balance between positive and negative charges is zero [48].When pH_{pzc} higher than pH, the surface of the adsorbent acquires a positive charge, consequently anions are attracted [49]. In contrast, when pH_{pzc} is lower than the pH, the surface of the adsorbent acquires a negative charge attracting cations. The pH of the adsorption essays was pH = 4 and the pH_{pzc} of CSNPS and BCS was 4.8 and 4.7, respectively, which implies an attraction of negatives charges of the dye in the surface of adsorbent in this research. Similar behavior was also reported by Verma et al. [50]. This parameter is a very important property because it is used to find the solution pH where the maximum pollutant removal is achieved [51]. Other studies made by Ngah, Fatinathan [52] found that the pH_{pzc} for BCS is at pH = 4 and informed by Ghiorghita et al. [53], the pH_{pzc} was equal to 4.95. Swelling degree (SD) was calculated to verify the water absorption capacity of the adsorbents. CSNPS (127.265%) obtained a higher SD than BCS (72.31%), and these values show a high-water absorption capacity because of the hydrophilic property of chitosan. Hydroxyl groups of chitosan have affinity for polar structures [20]. The difference of SD between the materials can be attributed to chitosan concentration, according to Poon et al. [54], the cross-linking is directly interrelated with swelling degree. The lower SD value for BCS may be related to excessive cross-linking and, consequently, higher stiffness [24]. Chaudhary et al. [55] reported that a high SD is a property that should possess an effective adsorbent for the decontamination of water, and this is ascertainable with the capacity adsorption result for nanoparticles and beads.

Kinetics

The kinetic models used to define the mechanism of adsorption of AR dye using BCS and CSNPs were pseudo-first order, pseudo-second order, and intraparticle diffusion. The constants of these models, as well as the calculated and experimental adsorption capacity at different concentration values, at pH = 4 and dry mass of 0.02 g for CSNPS and 0.25 g for BCS are presented in Table 5.

Tables 5 and 6 show that the adsorption capacity of BCS and CSNPS increases as the dye concentration increases.

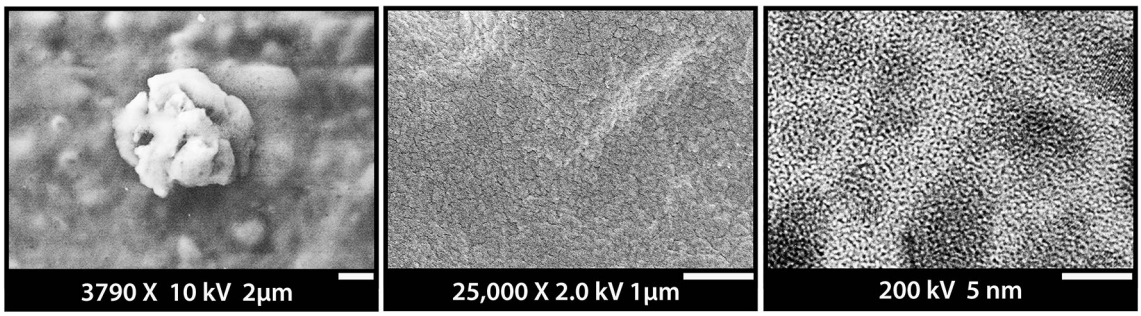

Fig. 4 SEM micrographs of BCS (**a**) and CSNPS (**b**). TEM micrographs for CSNPS (**c**)

Table 5 Kinetic parameters of pseudo-first order, pseudo-second order and intraparticle diffusion obtained from AR adsorption at different concentrations using CSNPS

CSNPS parameters	q_e (mg g^{-1})	Pseudo first order			Pseudo second order			Intraparticle diffusion	
		$q_{c\ (mg\ g^{-1})}$	$k_{1\ (min^{-1})}$	R^2	$q_{c\ (mg\ g^{-1})}$	$k_{2\ (mg\ min\ g^{-1})}$	R^2	$k_{1\ (mg\ min^{1/2}\ g^{-1})}$	R^2
Concentration (mg L^{-1})									
10	26.100	1.529	0.068	0.710	26.385	0.359	1	0.215	0.915
25	65.310	6.610	0.280	0.754	67.114	0.062	1	2.120	0.689
40	104.147	53.223	0.286	0.978	109.890	0.010	0.999	7.498	0.928
60	159.640	166.188	0.142	0.963	181.818	0.001	0.994	18.044	0.866
100	243.411	119.895	0.006	0.924	243.902	0.00025	1	4.341	0.749
150	328.244	208.833	0.003	0.955	344.828	0.000036	0.984	7.651	0.828
200	366.852	204.268	0.003	0.936	370.37	0.000048	0.995	7.220	0.915

Conditions of the AR solution: pH = 4, dry weight of adsorbent CSNPS = 0.02 g

Table 6 Kinetic parameters of pseudo-first order, pseudo-second order and intraparticle diffusion obtained from AR adsorption at different concentrations using BCS

BCS parameters	q_e (mg g^{-1})	Pseudo-first order			Pseudo-second order			Intraparticle diffusion	
		$q_{c\ (mg\ g^{-1})}$	$k_{1\ (min^{-1})}$	R^2	$q_{c\ (mg\ g^{-1})}$	$k_{2\ (mg\ min\ g^{-1})}$	R^2	$k_{1\ (mg\ min^{1/2}\ g^{-1})}$	R^2
Concentration (mg L^{-1})									
25	5.00	0.124	0.009	0.777	5.020	0.144	1.000	0.006	0.745
35	6.940	6.346	0.017	0.584	7.262	0.006	0.995	0.081	0.786
50	9.990	0.441	0.000	0.476	9.960	0.015	0.999	0.001	0.582
65	12.950	4.140	0.061	0.982	10.299	0.008	1.000	0.221	0.655
80	13.060	4.545	0.007	0.740	13.661	0.002	0.994	0.167	0.856
100	16.250	5.093	0.160	0.298	16.474	0.001	0.970	0.193	0.514

Conditions of the AR solution: pH = 4, dry weight of adsorbent BCS = 0.25 g

This could be because at low concentrations, there are more adsorption sites available to capture dye molecules. This phenomenon was also observed by Gonçalves et al. [56]. Once superficial diffusion of the dye that occurring on the surface of the active sites of the pores has ended, diffusion to the internal sites of the adsorbent begins. At this point, there is less availability of active sites, resulting in a longer time required for adsorption to occur.

Figure 5 describes the procedure of the production of the adsorbent structure and the interaction with the dye. In the first step, (Fig. 5a) is the initial interaction between the polymer (CS) and the cross-linker (TPP). This step present CS as a continuous chain polymer, and TPP as a frees ions agent cross-linker around the solution. In the second step (Fig. 5b), the reaction of cross-linking was accomplished, and the formation of the adsorbent was completed, during this process, the amino ($–NH_2$) groups of the polymer were protonated in acidic medium ($–NH_2$ to $+NH_3$) and by electrostatic forces, they were attached with the negative groups of the sodium tripolyphosphate (PO_4^-) forming a network (CSNPS and BCS). In the third step (Fig. 5c), it is the interaction between the adsorbent and the dye. The electrostatic forces involved causing an attraction between the existing positive groups of chitosan and the sulfonic negatives groups of the dye (SO_3^-). Shajahan et al. [57] and Sadiq et al. [58] also imply that this interaction occurs and affirm that, under acidic conditions, there is a positive ion surplus, which favors protonation of the amino groups in the main chitosan chain and increases the adsorption of the dye, as the electrostatic forces create an attraction between these groups and the sulfonic groups in the dye.

After the fitting of the experimental data was completed, the pseudo-second-order model best described the process of adsorption of AR on BCS and CSNPS, which confirms that it is a chemisorption and indicates the formation of a chemical bond resulting from electron exchange. Similar phenomena were reported by Wang et al. [18] and Tsotetsi et al. [47]. The validity of the model was determined by an R^2 value of 1 or close to 1 for all concentrations used in this study. Furthermore, the calculated adsorption capacity values (q_c = mg g^{-1}) were like the experimental adsorption capacity values.

The adsorption capacity values obtained from the adsorbent CSNPS were higher than those obtained from BCS, at

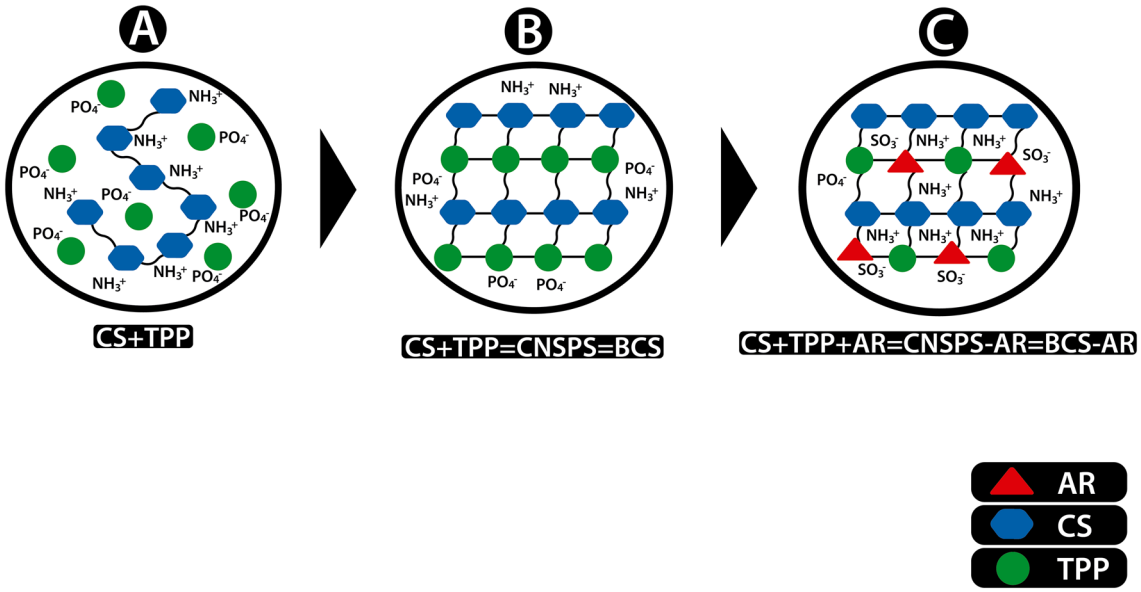

Fig. 5 Procedure of the reaction of cross-linking of the adsorbent and the adsorption reaction of the Allura Red dye on BCS and CSNPS. *AR* Allura rey dye, *CS* chitosan and *TPP* sodium tripolyphosfate

all concentrations used. The adsorption capacity is directly proportional to the concentration of the dye (the higher the concentration, the higher the adsorption capacity). Additionally, when the adsorption capacity increases, the contact time also increases. In this study, 0.02 g of CSNPS and 2.5 g of BCS, comparison (1–125) was used to enhance the adsorption capacity and optimize the required quantity (mass) of the adsorbent. The use of nanomaterials is beneficial because they have a larger contact area than other types of adsorbents [34]. Therefore, less adsorbent is required.

Considering the data obtained from the pseudo-second-order model as a reference (Table 6), it is observed that the adsorption rate k_2 (mg min^{-1} g^{-1}) for BCS and CSNPS decreases as the concentration increases (BCS from 0.144 to 0.001 mg min^{-1} g^{-1} and CSNPS from 0.359 to $4.8E^{-5}$ mg min^{-1} g^{-1}). Nanoparticles provide a higher surface area and availability of adsorption sites than beads and, as a result, their adsorption rate is higher.

In contrast, after analysis of the data obtained from the intraparticle diffusion model, it was noted that most of the calculated data did not fit the experimental data, with R^2 values ranging from 0.928 to 0.689; the adsorption rates did not show a constant behavior. Therefore, it was concluded that this model is not suitable for explaining the adsorption process for both adsorbent types.

In Table 6, it is shown that the pseudo-first-order model is more suitable than the intraparticle diffusion model. However, the fit is not better than pseudo second order (pseudo second order > pseudo first order > intraparticle diffusion) as represented by R^2 values. This indicates that mass transfer adsorption is not predominant for the adsorbents (BCS, CSNPS) used in this study.

Isotherms

Equilibrium models describe the phenomenon that prevails in the retention of substances from an aqueous to a solid phase at a constant temperature and pH [59]. In this work, experimental data were fitted to Langmuir, Freundlich, Dubinin–Raduskevich, Tempkin, and Redlich–Peterson isotherms. The obtained values of the parameters for each equilibrium model are listed in Table 7, also the values of the coefficient of determination (R^2) for each adsorption isotherm model are shown in bold.

The coefficient of determination (R^2) and chi-square (X^2) values, obtained for CSPNS and BCS from the Langmuir isotherm, behave similarly. This indicates that the process of adsorption in BCS and CSNPS occurs in the same way, regardless of particle size. However, the maximum adsorption capacity is significantly higher for CSPNS (320.5–370.37 mg g^{-1}) than for BCS (12.494–13.6 mg g^{-1}). Bevziuk et al. [15] state that the maximum adsorption capacity for dye molecules depends on the geometrical dimensions and spatial configuration of the adsorbent. This proves that the adsorption capacity of a dye decreases as particle size of the adsorbent increases. This is because either the dye cannot penetrate the particle of the adsorbent particle or it remains on its surface[60]. Additionally, the adsorption capacity is improved for both BCS and CSNPS, compared to similar studies [61, 62]. This is because the adsorbents used in this study were produced from chitosan with a high degree

Table 7 Results of variables of adsorption isotherms of Allura Red dye using chitosan beads and nanoparticles cross-linked with Sodium Tripolyphosphate (CSNPS)

Isotherm	Parameters	CSNPS			BCS		
		Linear	No linear		Linear	No linear	
		R^2	R^2	X^2	R^2	R^2	X^2
Langmuir	Q_{max} (mg g^{-1})	370.370	320.510	2422.397	13.600	12.494	5.157
	b (L mg^{-1})	0.711	2.153		2.730	7.486	
	R^2	**0.993**	**0.860**		**0.999**	**0.812**	
Freundlich	n	3.419	4.283	1019.652	6.900	7.511	2.853
	K_f (mg g^{-1})	130.380	146.894		8.850	9.028	
	R^2	**0.862**	**0.941**		**0.769**	**0.772**	
Dubinin–Raduskevich	Q_s (mg g^{-1})	258.320	305.412	3791.616	11.237	11.970	5.798
	K_{ad} (mol^2 kJ^2)	3.0E−08	6.0E−08		1.0E−08	1.9E−08	
	E	4082.483	2880.323		7071.068	5129.892	
	R^2	**0.876**	**0.781**		**0.497**	**0.537**	
Tempkin	A_t (L mg^{-1})	68.311	68.300	894.269	1148.026	1147.835	2.600
	B_t	58.355	42.478		1861.125	1861.125	
	B (J mol^{-1})	42.478	58.355		1.332	1.332	
	R^2	**0.957**	**0.948**		**0.883**	**0.792**	
Redlich–Peterson	A_r (L mg^{-1})	2.6E+08	3.2E+10	1284.709	1.6E+11	2.7E+11	3.805
	g	0.675	0.766		0.853	0.867	
	K_r (L g^{-1})	3.1E+10	4.7E+12		4.00E+12	2.4E+12	
	R^2	**0.985**	**0.926**		**0.991**	**0.696**	

of deacetylation (92.16%), which promotes the formation of H^+ bonds between some of the elements in the AR molecule (N, S, O, and C_6H_6) and the $–CH_2OH$ groups in the chitosan molecule, via hydrogen bonds or van der Waals forces [17]. A high degree of deacetylation provides a greater number of amino groups, which are able to protonate in acidic media, facilitating a better adsorption [63, 64]. This investigation it is shown how CSNPS and BCS are effective adsorbents to AR compared with others enlisted in Table 1.

Table 6 and Fig. 6 show that the best correlations of the adsorption models for CSNPS are in the following order: Tempkin > Redlich–Peterson > Langmuir > Freundlich > Dubinin–Raduskevich. The values of the coefficient of determination (R^2) (which were calculated using linear and nonlinear methods for Allura Red dye on CSNPS and BCS) showed values above 0.9 in all five analyzed isotherms. The lowest values of χ^2 were used to determine the best adsorption model. The Tempkin isotherm was the best model for CSNPS, and the Langmuir isotherm was the best for BCS, as these isotherms showed the highest R^2 values and the lowest χ^2 values. For CSNPS, this indicates that there are direct correlations between the adsorbate and adsorbent that are related to the maximum heat of adsorption, and it is expected that a uniform distribution will occur

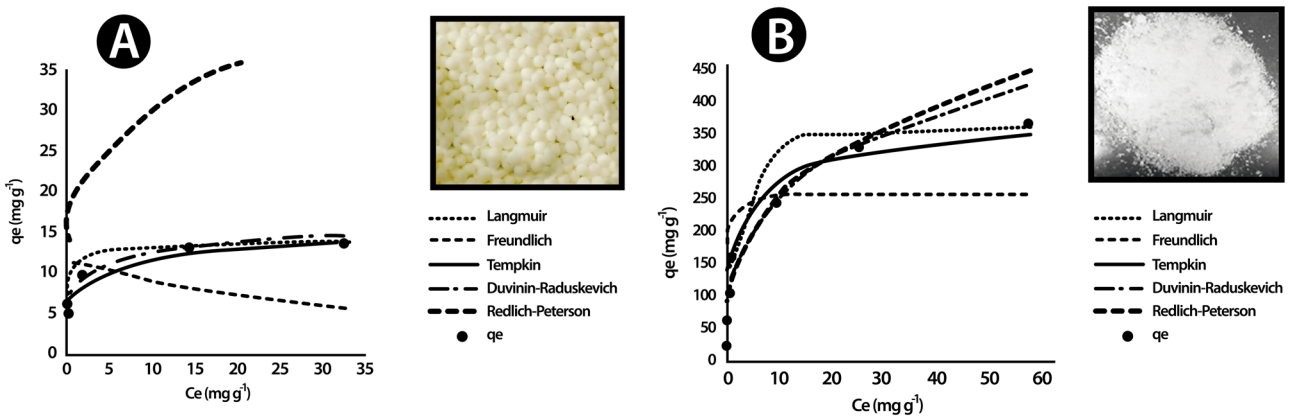

Fig. 6 Isotherms of adsorption of **a** BCS and **b** CSNPS

Table 8 Studies on adsorption of dyes using modified chitosan as adsorbent

Adsorbent	Particle size	Dye	Isotherm	References
Chitosan	0.10–26 mm	Red No. 40	Langmuir Redlich–Peterson	[8]
Chitosan/polyamide nanofiber	100–500 nm	Reactive Black 5 Ponceau 4R	Langmuir	[70]
Micro-nanofibrous chitosan sponges	86 nm	Acid Blue-113	Langmuir	[56]
Poly (AA-co-VPA) hydrogel cross-linked with *N*-maleyl chitosan	–	Methylene Blue Crystal Violet	Langmuir Redlich–Peterson	[71]
Chitosan film	–	Acid red 18 and FD&C blue no. 2	Redlich–Peterson	[72]
Cross-linked chitosan/oil palm ash composite beads	–	Reactive Blue 19	Redlich–Peterson	[18]
Fungal nanoparticles	2–30 nm	Brilliant Blue, Methyl Orange Disperse Red Naphthol Blue Black Chicago Sky Blue 6 B	Langmuir	[61]

as energetic bonds are generated [59, 65]. The best model to explain the adsorption process on BCS is the Langmuir model. It is noted that in the Redlich–Peterson model, the values of the g constant were close to 1. This indicates that the adsorption can also be explained by the Langmuir model in its linear form (CSNPS, $R^2 = 0.993$; BCS, $R^2 = 0.999$) where a monolayer adsorption with constant energy values occurs.

In contrast, the Dubinin–Raduskevich model for Allura Red on CSNPS and BCS had the lowest values of R^2 and the highest values of χ^2. Therefore, the mechanism of adsorption with a Gaussian distribution of the energy on a heterogeneous surface can be excluded [66]. Consequently, the mechanisms of Tempkin isotherm for CSNPS and Langmuir for BCS are confirmed. The RL factor of the Langmuir isotherm indicates a favorable adsorption process ($0 < R_L < 1$) for both adsorbents used. Ho, Ofomaja [67] indicated that the adsorption of dye-chitosan nanoparticles is compatible with the Langmuir model and the order of attraction forces is TPP > H_3O^+ > SO_3^- > hydrogen bonding under acidic conditions occurs.

In this study, it was concluded that anionic dyes such as Allura Red dye are adsorbed by ionic bonding and electrostatic interactions. Piccin et al. [68] found that Langmuir and Redlich–Peterson isotherms best describe the behavior of AR adsorption on chitosan; similar findings were reported by C [69]. A summary of relevant studies on adsorption processes, where chitosan was used as the adsorbent matrix, is shown in Table 8 as a complement of the background of this study.

Conclusions

The adsorption system was evaluated using two adsorbents: CSNPS and BCS. The adsorption essays were tested at acidic conditions (pH = 4). The adsorbents were characterized by FTIR, SEM, and TEM. The cross-linking of the TPP and the adsorption of AR were proved by FTIR. Also, swelling degree and potential zero charge were determined for both adsorbents. The pH_{pzc} was adequate for CSNPS and BCS in 4.8 and 4.7, respectively, supporting the attraction of negative charges of the dye. The particle size of the adsorbents was crucial in increasing the adsorption of the anionic dye, Allura Red. CSNPS exhibited a significantly higher adsorption capacity ($q_{max} = 370.37$ mg g^{-1}) than that of the BCS ($q_{max} = 13.60$ mg g^{-1}). Furthermore, CSNPS adsorbent mass was 125 times smaller than that of beads. The Tempkin isotherm model had the best fit for the nanoparticle adsorbent (CSNPS), while the Langmuir isotherm was the most suitable for BCS. It was suggested that in both cases, there is a monolayer adsorption with constant energy levels. An error analysis applying the nonlinear method permitted a more precise discernment of the isotherm model. Chemisorption by an equation of pseudo-second-order rate predominated as the adsorption mechanism of the dye on both adsorbents (BCS, CSNPS). The results of this research showed that the adsorption is possible under acidic conditions and with different concentrations of dye.

Acknowledgements This work was sponsored by Instituto Tecnologico de Sonora PROFAPI_2022_0490 and PROFAPI_2022_0512 project. The first author would like to give special thanks to CONACYT (269728) for all their support.

Declarations

Conflict of interest On behalf of all authors, the corresponding author states that there is no conflict of interest.

References

1. Abramsson-Zetterberg L, Ilbäck N-G (2013) The synthetic food colouring agent Allura Red AC (E129) is not genotoxic in a flow cytometry-based micronucleus assay in vivo. Food Chem Toxicol 59:86–89. https://doi.org/10.1016/j.fct.2013.05.047

2. Torres-Perez J, Huang Y, Bazargan A, Khoshand A, McKay G (2020) Two-stage optimization of Allura direct red dye removal by treated peanut hull waste. SN Appl Sci 2(3):475. https://doi.org/10.1007/s42452-020-2196-3
3. Blackburn RS, Harvey A (2004) Green chemistry methods in sulfur dyeing: application of various reducing D-sugars and analysis of the importance of optimum redox potential. Environ Sci Technol 38(14):4034–4039. https://doi.org/10.1021/es0498484
4. Nakhjiri MT, Marandi GB, Kurdtabar M (2018) Poly(AA-co-VPA) hydrogel cross-linked with N-maleyl chitosan as dye adsorbent: isotherms, kinetics and thermodynamic investigation. Int J Biol Macromol 117:152–166. https://doi.org/10.1016/j.ijbiomac.2018.05.140
5. Haldorai Y, Kharismadewi D, Tuma D, Shim J-J (2015) Properties of chitosan/magnetite nanoparticles composites for efficient dye adsorption and antibacterial agent. Korean J Chem Eng 32(8):1688–1693. https://doi.org/10.1007/s11814-014-0368-9
6. Dotto GL, Santos JMN, Tanabe EH, Bertuol DA, Foletto EL, Lima EC, Pavan FA (2017) Chitosan/polyamide nanofibers prepared by Forcespinning® technology: a new adsorbent to remove anionic dyes from aqueous solutions. J Clean Prod 144:120–129. https://doi.org/10.1016/j.jclepro.2017.01.004
7. Salem MA, Elsharkawy RG, Ayad MI, Elgendy MY (2019) Silver nanoparticles deposition on silica, magnetite, and alumina surfaces for effective removal of Allura red from aqueous solutions. J Sol Gel Sci Technol 91(3):523–538. https://doi.org/10.1007/s10971-019-05055-7
8. Piccin JS, Vieira MLG, Gonçalves JO, Dotto GL, Pinto LAA (2009) Adsorption of FD&C Red No. 40 by chitosan: isotherms analysis. J Food Eng 95(1):16–20. https://doi.org/10.1016/j.jfoodeng.2009.03.017
9. Mondal S, Bobde K, Aikat K, Halder G (2016) Biosorptive uptake of ibuprofen by steam activated biochar derived from mung bean husk: equilibrium, kinetics, thermodynamics, modeling and ecotoxicological studies. J Environ Manag 182:581–594. https://doi.org/10.1016/j.jenvman.2016.08.018
10. Nabavi SM, Silva AS (2018) Chitosan. In: Nonvitamin and nonmineral nutritional supplements. Academic Press
11. Azevedo JR, Sizilio RH, Brito MB, Costa AMB, Serafini MR, Araújo AAS, Santos MRV, Lira AAM, Nunes RS (2011) Physical and chemical characterization insulin-loaded chitosan-TPP nanoparticles. J Therm Anal Calorim 106(3):685–689. https://doi.org/10.1007/s10973-011-1429-5
12. Okamoto-Schalch NO, Pinho SGB, de Barros-Alexandrino TT, Dacanal GC, Assis OBG, Martelli-Tosi M (2020) Production and characterization of chitosan-TPP/cellulose nanocrystal system for encapsulation: a case study using folic acid as active compound. Cellulose 27(10):5855–5869. https://doi.org/10.1007/s10570-020-03173-y
13. Hasan M, Ahmad AL, Hameed BH (2008) Adsorption of reactive dye onto cross-linked chitosan/oil palm ash composite beads. Chem Eng J 136(2):164–172. https://doi.org/10.1016/j.cej.2007.03.038
14. Foruzin LJ, Rezvani Z, Nejati K (2018) Preparation of two-color photoluminescence emission based on azo dye-layered double hydroxide systems and controlling photoluminescence properties of Allura Red AC. J Iran Chem Soc 15(12):2649–2658. https://doi.org/10.1007/s13738-018-1453-5
15. Bevziuk K, Chebotarev A, Koicheva A, Snigur D (2018) Adsorption of anionic food azo dyes from aqueous solution by silica modified with cetylpyridinium chloride. Monat Chem Chem Mon 149(12):2153–2160. https://doi.org/10.1007/s00706-018-2301-0
16. Sadegh H, Ali GAM, Gupta VK, Makhlouf ASH, Shahryari-ghoshekandi R, Nadagouda MN, Sillanpää M, Megiel E (2017) The role of nanomaterials as effective adsorbents and their applications in wastewater treatment. J Nanostruct Chem 7(1):1–14. https://doi.org/10.1007/s40097-017-0219-4
17. Kacem SB, Elaoud SC, Asensio AM, Panizza M, Clematis D (2021) Electrochemical and sonoelectrochemical degradation of Allura Red and Erythrosine B dyes with Ti-PbO_2 anode. J Electroanal Chem 889:115212. https://doi.org/10.1016/j.jelechem.2021.115212
18. Wang H, Li Z, Yahyaoui S, Hanafy H, Seliem MK, Bonilla-Petriciolet A, Luiz Dotto G, Sellaoui L, Li Q (2021) Effective adsorption of dyes on an activated carbon prepared from carboxymethyl cellulose: experiments, characterization and advanced modelling. Chem Eng J 417:128116. https://doi.org/10.1016/j.cej.2020.128116
19. Herrera-García S, Aguirre-Ramírez M, Torres-Pérez J (2020) Comparison between Allura Red dye discoloration by activated carbon and azo bacteria strain. Environ Sci Pollut Res 27(23):29688–29696. https://doi.org/10.1007/s11356-020-09584-5
20. Schio RR, Gonçalves JO, Mallmann ES, Pinto D, Dotto GL (2021) Development of a biosponge based on *Luffa cylindrica* and crosslinked chitosan for Allura red AC adsorption. Int J Biol Macromol 192:1117–1122. https://doi.org/10.1016/j.ijbiomac.2021.10.096
21. Ávila-Martínez AK, Roque-Ruiz JH, Torres-Pérez J, Medellín-Castillo NA, Reyes-López SY (2020) Allura Red dye sorption onto electrospun zirconia nanofibers. Environ Technol Innov 18:100760. https://doi.org/10.1016/j.eti.2020.100760
22. Sánchez-Duarte RG, Sánchez-Machado DI, López-Cervantes J, Correa-Murrieta MA (2012) Adsorption of allura red dye by cross-linked chitosan from shrimp waste. Water Sci Technol 65(4):618–623. https://doi.org/10.2166/wst.2012.900
23. Langmuir I (1916) The constitution and fundamental properties of solids and liquids. Part I. Solids. J Am Chem Soc 38(11):2221–2295. https://doi.org/10.1021/ja02268a002
24. Sharma B, Thakur S, Mamba G, Prateek, Gupta RK, Gupta VK, Thakur VK (2021) Titania modified gum tragacanth based hydrogel nanocomposite for water remediation. J Environ Chem Eng 9(1):104608. https://doi.org/10.1016/j.jece.2020.104
25. Gonçalves JO, Santos JP, Rios EC, Crispim MM, Dotto GL, Pinto LAA (2017) Development of chitosan based hybrid hydrogels for dyes removal from aqueous binary system. J Mol Liq 225:265–270. https://doi.org/10.1016/j.molliq.2016.11.067
26. Sharma B, Thakur S, Trache D, Yazdani Nezhad H, Thakur VK (2020) Microwave-assisted rapid synthesis of reduced graphene oxide-based gum tragacanth hydrogel nanocomposite for heavy metal ions adsorption. Nanomaterials 10(8):1616
27. Freundlich H (1907) Über die adsorption in Lösungen. Z Phys Chem. https://doi.org/10.1515/zpch-1907-5723
28. Kaušpėdienė D, Kazlauskienė E, Gefenienė A, Binkienė R (2010) Comparison of the efficiency of activated carbon and neutral polymeric adsorbent in removal of chromium complex dye from aqueous solutions. J Hazard Mater 179(1):933–939. https://doi.org/10.1016/j.jhazmat.2010.03.095
29. Ho Y-S (2006) Review of second-order models for adsorption systems. J Hazard Mater 136(3):681–689. https://doi.org/10.1016/j.jhazmat.2005.12.043
30. Foo KY, Hameed BH (2010) Insights into the modeling of adsorption isotherm systems. Chem Eng J 156(1):2–10. https://doi.org/10.1016/j.cej.2009.09.013
31. Shirmardi M, Mahvi AH, Mesdaghinia A, Nasseri S, Nabizadeh R (2013) Adsorption of acid red18 dye from aqueous solution using single-wall carbon nanotubes: kinetic and equilibrium. Desalination Water Treat 51(34–36):6507–6516. https://doi.org/10.1080/19443994.2013.793915

32. Bergaoui M, Nakhli A, Benguerba Y, Khalfaoui M, Erto A, Soetaredjo FE, Ismadji S, Ernst B (2018) Novel insights into the adsorption mechanism of methylene blue onto organo-bentonite: adsorption isotherms modeling and molecular simulation. J Mol Liq 272:697–707. https://doi.org/10.1016/j.molliq.2018.10.001
33. Temkin MaP V (1940) Kinetics of ammonia synthesis on promoted iron catalysts. Acta Physicochim URSS 12:217–222
34. Chan LSCWH, Allen SJ, McKay G (2012) Error analysis of adsorption isotherm models for acid dyes onto Bamboo derived actived carbon. Chin J Chem Eng 20(3):535–542
35. Alver E, Bulut M, Metin AÜ, Çiftçi H (2017) One step effective removal of Congo Red in chitosan nanoparticles by encapsulation. Spectrochim Acta Part A Mol Biomol Spectrosc 171:132–138. https://doi.org/10.1016/j.saa.2016.07.046
36. Correa-Murrieta MA, López-Cervantes J, Sánchez-Machado DI, Sánchez-Duarte RG, Rodríguez-Núñez JR, Núñez-Gastélum JA (2012) Fe(II) and Fe(III) adsorption by chitosan-tripolyphosphate beads: kinetic and equilibrium studies. J Water Supply Res Technol Aqua 61(6):331–341. https://doi.org/10.2166/aqua.2012.048
37. Gimbert F, Morin-Crini N, Renault F, Badot P-M, Crini G (2008) Adsorption isotherm models for dye removal by cationized starch-based material in a single component system: error analysis. J Hazard Mater 157(1):34–46. https://doi.org/10.1016/j.jhazmat.2007.12.072
38. Figueroa D, Moreno A, Hormaza A (2015) Equilibrio, termodinámica y modelos cinéticos en la adsorción de Rojo 40 sobre tuza de maíz. Rev Ing Univ Medel 14:105–120
39. Ho YS, McKay G (1999) The sorption of lead(II) ions on peat. Water Res 33(2):578–584. https://doi.org/10.1016/S0043-1354(98)00207-3
40. Chakraborty P, Show S, Ur Rahman W, Halder G (2019) Linearity and non-linearity analysis of isotherms and kinetics for ibuprofen remotion using superheated steam and acid modified biochar. Process Saf Environ Prot 126:193–204. https://doi.org/10.1016/j.psep.2019.04.011
41. Loutfy SA, Alam El-Din HM, Elberry MH, Allam NG, Hasanin MTM, Abdellah AM (2016) Synthesis, characterization and cytotoxic evaluation of chitosan nanoparticles: *in vitro* liver cancer model. Adv Nat Sci Nanosci Nanotechnol 7(3):035008. https://doi.org/10.1088/2043-6262/7/3/035008
42. Khan M, Khan A, Khan H, Ali N, Sartaj S, Malik S, Ali N, Khan H, Shah S, Bilal M (2021) Development and characterization of regenerable chitosan-coated nickel selenide nano-photocatalytic system for decontamination of toxic azo dyes. Int J Biol Macromol 182:866–878. https://doi.org/10.1016/j.ijbiomac.2021.03.192
43. Al Shamari YMG, Al-Warthan AA, Wabaidur SM, Khan MA, Alqadami AA, Siddiqui MR (2020) New Ultra Performance liquid chromatography-mass spectrometric method for the determination of allura red in soft drinks using corncob as solid phase extraction sorbent: analysis and food waste management approach. J King Saud Univ Sci 32:1135–1141
44. Zeng W, Hui H, Liu Z, Chang Z, Wang M, He B, Hao D (2021) TPP ionically cross-linked chitosan/PLGA microspheres for the delivery of NGF for peripheral nerve system repair. Carbohydr Polym 258:117684. https://doi.org/10.1016/j.carbpol.2021.117684
45. Thirumalaikumar E, Lelin C, Sathishkumar R, Vimal S, Anand SB, Babu MM, Citarasu T (2021) Oral delivery of pVAX-OMP and pVAX-hly DNA vaccine using chitosan-tripolyphosphate (Cs-TPP) nanoparticles in Rohu, (Labeo rohita) for protection against Aeromonas hydrophila infection. Fish Shellfish Immunol 115:189–197. https://doi.org/10.1016/j.fsi.2021.06.004
46. Villegas-Peralta Y, Lopez-Cervantes J, Santana T, Sanchez-Duarte RG, Sánchez-Machado D, Martínez Macias MDR, Correa-Murrieta M (2021) Impact of the molecular weight on the size of chitosan nanoparticles: characterization and its solid-state application. Polym Bull. https://doi.org/10.1007/s00289-020-03139-x
47. Tsotetsi D, Dhlamini M, Mbule P (2022) Sol-gel derived mesoporous TiO_2: effects of non-ionic co-polymers on the pore size, morphology, specific surface area and optical properties analysis. Results Mater 14:100266. https://doi.org/10.1016/j.rinma.2022.100266
48. Thakur S, Arotiba O (2018) Synthesis, characterization and adsorption studies of an acrylic acid-grafted sodium alginate-based TiO_2 hydrogel nanocomposite. Adsorpt Sci Technol 36(1–2):458–477. https://doi.org/10.1177/0263617417700636
49. Vences-Alvarez E, Chazaro-Ruiz LF, Rangel-Mendez JR (2022) New bimetallic adsorbent material based on cerium-iron nanoparticles highly selective and affine for arsenic(V). Chemosphere 297:134177. https://doi.org/10.1016/j.chemosphere.2022.134177
50. Verma A, Thakur S, Mamba G, Prateek, Gupta RK, Thakur P, Thakur VK (2020) Graphite modified sodium alginate hydrogel composite for efficient removal of malachite green dye. Int J Biol Macromol 148:1130–1139. https://doi.org/10.1016/j.ijbiomac.2020.01.142
51. Medellín-Castillo NA, Isaacs-Páez ED, Rodríguez-Méndez I, González-García R, Labrada-Delgado GJ, Aragón-Piña A, García-Arreola ME (2021) Formaldehyde and tripolyphosphate crosslinked chitosan hydrogels: synthesis, characterization and modeling. Int J Biol Macromol 183:2293–2304. https://doi.org/10.1016/j.ijbiomac.2021.06.020
52. Ngah WSW, Fatinathan S (2010) Adsorption characterization of Pb(II) and Cu(II) ions onto chitosan-tripolyphosphate beads: kinetic, equilibrium and thermodynamic studies. J Environ Manag 91(4):958–969. https://doi.org/10.1016/j.jenvman.2009.12.003
53. Ghiorghita C-A, Borchert KBL, Vasiliu A-L, Zaharia M-M, Schwarz D, Mihai M (2020) Porous thiourea-grafted-chitosan hydrogels: Synthesis and sorption of toxic metal ions from contaminated waters. Colloids Surf A: Physicochem Eng Asp 607:125504. https://doi.org/10.1016/j.colsurfa.2020.125504
54. Poon L, Wilson LD, Headley JV (2014) Chitosan-glutaraldehyde copolymers and their sorption properties. Carbohydr Polym 109:92–101. https://doi.org/10.1016/j.carbpol.2014.02.086
55. Chaudhary J, Thakur S, Mamba G, Prateek, Gupta RK, Thakur VK (2021) Hydrogel of gelatin in the presence of graphite for the adsorption of dye: Towards the concept for water purification. J Environ Chem Eng 9(1):104762. https://doi.org/10.1016/j.jece.2020.104762
56. Gonçalves JO, Silva KA, Dotto GL, Pinto LAA (2018) Adsorption kinetics of dyes in single and binary systems using cyanoguanidine-crosslinked chitosan of different deacetylation degrees. J Polym Environ 26(6):2401–2409. https://doi.org/10.1007/s10924-017-1133-z
57. Shajahan A, Shankar S, Sathiyaseelan A, Narayan KS, Narayanan V, Kaviyarasan V, Ignacimuthu S (2017) Comparative studies of chitosan and its nanoparticles for the adsorption efficiency of various dyes. Int J Biol Macromol 104(Part C):1449–1458. https://doi.org/10.1016/j.ijbiomac.2017.05.128
58. Sadiq AC, Olasupo A, Rahim NY, Ngah WSW, Suah FBM (2021) Comparative removal of malachite green dye from aqueous solution using deep eutectic solvents modified magnetic chitosan nanoparticles and modified protonated chitosan beads. J Environ Chem Eng 9(5):106281. https://doi.org/10.1016/j.jece.2021.106281
59. Saruchi KV (2019) Adsorption kinetics and isotherms for the removal of rhodamine B dye and Pb^{+2} ions from aqueous solutions by a hybrid ion-exchanger. Arab J Chem 12(3):316–329. https://doi.org/10.1016/j.arabjc.2016.11.009
60. Manuela Mincea VP, Negrulescu A, Szabo R, Ostafe V (2013) Adsorption of Three commercial dyes onto chitosan beads using spectrophotometric determination and a multivariate calibration

method. J Water Resour Prot 5(4):446–457. https://doi.org/10.4236/jwarp.2013.54044
61. Shajahan A, Shankar S, Sathiyaseelan A, Narayan KS, Narayanan V, Kaviyarasan V, Ignacimuthu S (2017) Comparative studies of chitosan and its nanoparticles for the adsorption efficiency of various dyes. Int J Biol Macromol 104:1449–1458. https://doi.org/10.1016/j.ijbiomac.2017.05.128
62. Shokrollahi A, Alizadeh A, Malekhosseini Z, Ranjbar M (2011) Removal of bromocresol green from aqueous solution via adsorption on *Ziziphus nummularia* as a new, natural, and low-cost adsorbent: kinetic and thermodynamic study of removal process. J Chem Eng Data 56:3738–3746. https://doi.org/10.1021/je200311y
63. Lee R-SJR-LTF-CWS-H (1999) Adsorption behavior of reactive dyes from aqueous solutions on chitosan
64. Juang R-S, Tseng R-L, Wu F-C, Lee S-H (1997) Adsorption behavior of reactive dyes from aqueous solutions on chitosan. J Chem Technol Biotechnol 70(4):391–399. https://doi.org/10.1002/(sici)1097-4660(199712)70:4%3c391::aid-jctb792%3e3.0.co;2-v
65. Sadeghi-Kiakhani M, Arami M, Gharanjig K (2013) Dye removal from colored-textile wastewater using chitosan-PPI dendrimer hybrid as a biopolymer: optimization. Kinetic Isotherm Stud. https://doi.org/10.1002/app.37615
66. Khaled A, Nemr AE, El-Sikaily A, Abdelwahab O (2009) Removal of Direct N Blue-106 from artificial textile dye effluent using activated carbon from orange peel: adsorption isotherm and kinetic studies. J Hazard Mater 165(1):100–110. https://doi.org/10.1016/j.jhazmat.2008.09.122
67. Ho Y-S, Ofomaja AE (2006) Pseudo-second-order model for lead ion sorption from aqueous solutions onto palm kernel fiber. J Hazard Mater 129(1):137–142. https://doi.org/10.1016/j.jhazmat.2005.08.020
68. Piccin J, Vieira MLG, Gonçalves J, Dotto G, Pinto L (2009) Adsorption of FD&C Red no 40 by chitosan: isotherms analysis. J Food Eng 95:16–20. https://doi.org/10.1016/j.jfoodeng.2009.03.017
69. Weber WJ Jr, Morris JC (1963) Kinetics of adsorption of carbon from solution. J Sanit Eng Div Am Soc Civ Eng 89(1):31–60
70. Tseng R-L, Wu F-C, Juang R-S (2010) Characteristics and applications of the Lagergren's first-order equation for adsorption kinetics. J Taiwan Inst Chem Eng 41(6):661–669. https://doi.org/10.1016/j.jtice.2010.01.014
71. Obeid L, Bée A, Talbot D, Jaafar SB, Dupuis V, Abramson S, Cabuil V, Welschbillig M (2013) Chitosan/maghemite composite: a magsorbent for the adsorption of methyl orange. J Colloid Interface Sci 410:52–58. https://doi.org/10.1016/j.jcis.2013.07.057
72. Zeraatkar Moghaddam A, Ghiamati E, Pourashuri A, Allahresani A (2018) Modified nickel ferrite nanocomposite/functionalized chitosan as a novel adsorbent for the removal of acidic dyes. Int J Biol Macromol 120:1714–1725. https://doi.org/10.1016/j.ijbiomac.2018.09.198